TSINGHUA SCIENCE AND TECHNOLOGY
ISSN 1007-0214 22/24 pp1593–1603
DOI: 10.26599/TST.2023.9010127
Volume 29, Number 5, October 2024

# Focusing Ability Enhancement in Broadside Direction of Array: From UCA to UCCA

Zidong Wu and Linglong Dai*

**Abstract:** To meet the ever-increasing demand for the data rates of wireless communications, extremely large-scale antenna array (ELAA) has emerged as one of the candidate technologies for future 6G communications. The significantly increased number of antennas in ELAA gives rise to near-field communications, necessitating tailored beamforming techniques within the near-field regions to accommodate the spherical-wave propagation characteristics. Among various array geometries of ELAA, uniform circular array (UCA) has gained much attention for its distinct capability of maintaining uniform beam pattern across different azimuth angles. However, existing analysis of near-field UCA beamforming indicates that the near-field region severely declines in the broadside of UCA, where the system fails to benefit from near-field communications. To tackle this problem, the near-field beamforming technique of uniform concentric circular arrays (UCCAs) is investigated in this paper, which has the potential to enlarge the near-field region in the broadside direction. First, the analysis of beamforming gain in the 3D space with UCA and UCCA is provided. Then, the distinct beamforming characteristics that set UCCA apart from UCA are delineated, revealing the superiority of UCCA in extending the near-field region in broadside at the cost of slightly reduced near-field region in the coplane. Simulation results are provided to verify the effectiveness of the theoretical analysis of beamforming gain with UCCA and the enhanced focusing ability of UCCA in the broadside direction.

**Key words:** extremely large-scale antenna array (ELAA); uniform concentric circular array (UCCA); near-field communications

## 1 Introduction

To satisfy the significantly increased requirements of wireless data transmissions, millimeter-wave (mmWave) and terahertz (THz) communications with extremely large-scale antenna array (ELAA) have been viewed as one of the candidate technologies for 6G communications. In comparison to 5G massive multiple-input multiple-output (MIMO), the integration of ELAA at the base station (BS) is promising to further improve the peak data rate and spectrum efficiency by harnessing higher beamforming gain and multiplexing gain through the employment of tenfold more antennas[1].

The substantial enlargement of the array aperture leads to the expanded near-field region within ELAA systems, indicating the probable prevalence of near-field communications in future 6G networks[2]. In near-field communications, the classical planar-wave propagation model in 5G massive MIMO systems is not accurate anymore, which needs to be replaced with the accurate spherical-wave propagation model. The transformation from planar-wave to spherical-wave

• Zidong Wu and Linglong Dai are with Department of Electronic Engineering, Tsinghua University, and also with Beijing National Research Center for Information Science and Technology (BNRist), Beijing 100084, China. E-mail: wuzd19@mails.tsinghua.edu.cn; daill@tsinghua.edu.cn.
* To whom correspondence should be addressed.
Manuscript received: 2023-08-27; revised: 2023-10-14; accepted: 2023-10-23

propagation model results in the mismatch of classical planar-wave-based techniques and actual spherical-wave-based channel models. This mismatch has substantially diminished the beamforming gain, thereby negatively impacting overall system performance[2].

To retrieve the beamforming loss, specific beamforming techniques tailored for near-field narrowband communications have been developed in Ref. [3]. The phase differences between antennas resulting from spherical-wave propagation were compensated with beamforming vectors to form expected constructive interference. When it comes to near-field wideband systems, a phase-delay focusing (PDF) method was designed to mitigate the near-field beam split effect, which originates from the fact that the frequency-independent phase shifters could not satisfy the requirement of frequency-dependent phase shifts. With the proposed PDF method, a high beamforming gain across the entire bandwidth could be ensured[4].

Different from the works aiming to retrieve the performance loss of far-field beamforming techniques in near-field region, the potential benefits of near-field beamforming were also investigated. Specifically, it was pointed out that, unlike far-field beamforming which only steers the signal in a desired direction, near-field beamforming with the spherical-wave propagation model is capable of simultaneously focusing signal energy on a specific direction and a specific distance[5]. Owing to its additional focusing ability in the distance domain, it was revealed that inter-user interferences could be better controlled with near-field beamforming in multi-user MIMO systems, which is promising to improve the spectrum efficiency performance[6]. The near-field precoding method leveraging the additional focusing ability in the distance domain was proposed to simultaneously serve multiple users in the same direction[7].

However, the aforementioned works exclusively concentrated on the geometry of uniform linear array (ULA). Despite the wide consideration of ULA, it was noted that the beam pattern of ULA experiences distortion in large angles deviated from the broadside direction[8]. Therefore, the service quality could not be ensured when users move to the edge of ULA. To overcome this drawback, uniform circular array (UCA) was designed to guarantee an unchanged beam pattern in far-field communications, which originates from its rotational symmetry property[8]. Considering the spherical-wave propagation, near-field beamforming with UCA was developed in Ref. [9], where the focusing ability of UCA in the distance domain was investigated. Nevertheless, the closed-form beamforming analysis was confined to an ideal two-dimensional (2D) scenario, which is hard to be satisfied in practical. Another work investigating the three-dimensional (3D) beamforming property of UCA with local approximation methods indicates that the focusing ability of UCA in the distance domain may decline in the broadside direction, where the benefits of near-field communication could not be harnessed[10].

To tackle this problem, the uniform concentric circular array (UCCA) is leveraged to enhance the focusing ability in the broadside direction in this paper. In existing works, UCCA was proposed in replacement of UCA due to its advantages in enabling a wider bandwidth for wideband communications[11] and generating higher beamforming gain in hybrid precoding communication schemes[12]. For instance, in Refs. [11] and [13], it was noticed that an increasing radius of UCA would result in a narrower passband. With a combination of arrays with different radii, UCCA could provide a balanced performance over a wider bandwidth since smaller circular arrays could compensate for the narrow passband of larger circular arrays. In addition, compared with UCA where antennas are only placed along the circular periphery, UCCA enables a tight spatial deployment method. Thus, more antennas could be deployed in the limited space at base station, where improved beamforming gain and multiplexing gain could be anticipated with UCCA. However, existing analysis of UCCA is mainly restricted to far-field communications. To the best of our knowledge, the near-field beamforming property of UCCA is rarely investigated, let alone revealing the potential advantages of UCCA in enhancing the focusing ability compared with UCA.

To fill in this gap, the near-field beamforming techniques employing UCCA are investigated in this paper. First, the 3D beamforming analysis with UCA is provided, revealing the phenomenon that the near-field region severely reduces in the broadside direction of UCA. Then, the near-field beam pattern of UCCA in the distance domain was investigated. Our analysis verifies that UCCA offers an enhanced focusing ability in the broadside direction while at the same time improves the space utilization efficiency. Furthermore,

with the improved focusing ability, UCCA is able to enlarge the near-field region in the broadside direction compared with UCA, providing the possibility to take advantage of the near-field effect to enhance system performance.

## 2 System Model

In this paper, we consider a downlink ELAA mmWave communication system, where the BS is equipped with a UCCA to serve single-antenna users. The radius of the $m^{\text{th}}$ UCA is denoted by $R_m$ for $m = 1, 2, \ldots, M$, in which $N_m$ omnidirectional antennas are uniformly distributed in different azimuth angles, as shown in Fig. 1. Thus, the coordinate of the $n^{\text{th}}$ antenna of the $m^{\text{th}}$ UCA can be expressed as $(R_m, \pi/2, \psi_n)$ in the spherical coordinate system, where $\psi_n = \dfrac{2\pi n}{N_m}$ for $n = 1, 2, \ldots, N_m$. In the cartesian coordinate system, the coordinate of the $n^{\text{th}}$ antenna of $m^{\text{th}}$ UCA could be expressed as $(R_m \cos\psi_n, R_m \sin\psi_n, 0)$. In addition, to ensure a uniform distribution of antennas, the radius of $m^{\text{th}}$ UCA is assumed to be proportional to the index $m$, i.e., $R_m = \dfrac{m}{M} R_{\max}$ and $N_m = \dfrac{m}{M} N_{\max}$ where $R_{\max}$ and $N_{\max}$ denote the radius and the number of antennas of the outermost UCA, respectively.

In massive MIMO mmWave systems, the channel between the $m^{\text{th}}$ UCA and user could be described as[14]

$$h_m = \sum_{l=1}^{L} g_l \, a_m(\theta_l, \phi_l) \tag{1}$$

where $L$ denotes the number of resolvable paths between BS and the user. Notations $g_l$, $\theta_l$, and $\phi_l$ denote the complex gain, elevation angle, and azimuth angle of the $l^{\text{th}}$ path, respectively. The beam steering vector $a_m(\theta, \phi)$ describes the single-path wave impinging on the $m^{\text{th}}$ UCA of UCCA from direction

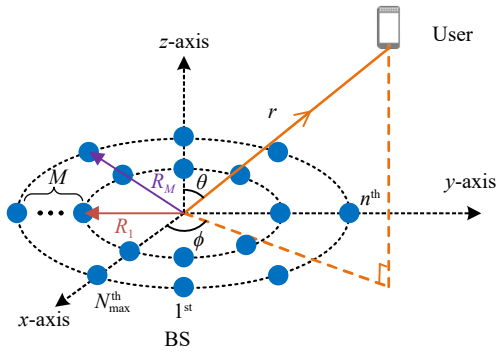


**Fig. 1 Array geometry of UCCA with a single-antenna user.**

$(\theta, \phi)$, expressed as

$$a_m(\theta, \phi) = \frac{1}{\sqrt{N}} \left[ e^{jkR_m \sin\theta\cos(\phi-\psi_1)}, \right.$$
$$\left. e^{jkR_m \sin\theta\cos(\phi-\psi_2)}, \ldots, e^{jkR_m \sin\theta\cos(\phi-\psi_{N_m})} \right]^{\mathrm{T}} \tag{2}$$

where $k = \dfrac{2\pi}{\lambda}$ and $N = \sum_{m=1}^{M} N_m$ denote the wavenumber and the total number of antennas of UCCA, respectively. The operator $(A)^{\mathrm{T}}$ denotes the transpose of matrix $A$. It is worth noting that the beam steering vector in Eq. (2) is derived with the planar-wave propagation model, which is valid in existing 5G massive MIMO systems where near-field communications are uncommon. However, due to the significantly enlarged array aperture of ELAA, the near-field region dramatically expands and users are likely to be located in the near-field region, where the spherical-wave propagation model has to be adopted instead. Consequently, the far-field beam steering vector based on planar-wave propagation models fails to characterize the spherical-wave propagation in ELAA systems.

To tackle the mismatch of propagation models, a more accurate near-field beam steering vector for UCA has been employed in Ref. [9], which is written as

$$b_m(r, \theta, \phi) = \frac{1}{\sqrt{N}} \left[ e^{-jk\left(r_m^{(1)} - r\right)}, \ldots, e^{-jk\left(r_m^{(N_m)} - r\right)} \right]^{\mathrm{T}} \tag{3}$$

where $r_m^{(n)}$ and $r$ denote the distance between user and $n^{\text{th}}$ antenna of the $m^{\text{th}}$ UCA and distance between user and the center of UCCA, respectively. The distance term $r_m^{(n)}$ could be written based on the law of cosines as

$$r_m^{(n)} = \sqrt{r^2 + R_m^2 - 2rR_m \sin\theta\cos(\phi - \psi_n)} \overset{(a)}{\approx}$$
$$r - R_m \sin\theta\cos(\phi - \psi_n) +$$
$$\frac{R_m^2}{2r}\left(1 - \sin^2\theta\cos^2(\phi - \psi_n)\right) \tag{4}$$

where approximation (a) is derived with the second-order Tylor series expansion. It is worth noting that the approximation is valid for most near-field communications systems[15, 16]. Specifically, with enlarged array aperture $D$ of ELAA, communications are likely to happen between the Rayleigh distance $r_{\mathrm{RD}} = 2D^2/\lambda$ and the Fresnel distance $r_{\mathrm{FD}} = D(D/\lambda)^{1/3}/2$. Formula (4) has been proved accurate between the Rayleigh distance and Fresnel distance in Ref. [15], which lays the foundation of the analysis of this paper.

With the beam steering vector in Eq. (3), the near-field beam steering vector for the whole UCCA could be constructed by concatenating near-field beam steering vectors for different UCAs, written as

$$b(r,\theta,\phi)=\left[b_1(r,\theta,\phi)^{\mathrm{T}},b_2(r,\theta,\phi)^{\mathrm{T}},\ldots,b_M(r,\theta,\phi)^{\mathrm{T}}\right]^{\mathrm{T}} \quad (5)$$

It is noteworthy that, different from the classical far-field beam steering vectors in Eq. (2) which are only determined by elevation angle $\theta$ and azimuth angle $\phi$[14], the near-field beam steering vector in Eq. (3) and Eq. (5) is also related to propagation distance $r$. The underlying relationship between far-field and near-field steering vectors lies in that if $r$ tends to infinity, the near-field beam steering vector in Eq. (3) will naturally degrade into the far-field beam steering vector in Eq. (2). Therefore, the near-field steering vector depicts a more general model embracing the far-field steering vector model as a special case.

Since the line-of-sight (LoS) component dominates mmWave and THz channels, the LoS component reflects most of the channel characteristics. Thus, the near-field beamforming property of UCCA with only LoS channels is investigated in this paper, revealing the distinguishing beamforming property of UCCA in near-field communications.

## 3 UCCA Near-Field Beamforming Analysis

### 3.1 3D beamforming with UCA

Since the beamforming property of UCCA is hard to be directly analyzed, we first consider a simplified model of UCCA, i.e., single UCA, for 3D beamforming analysis. The number of antennas and radius of UCA are thereby expressed as $N=N_m$ and $R_{\max}=R_m$, respectively. Adopting the widely-employed matched-filter method to perform beamforming, the beamforming vector could be selected as the conjugate transpose of the beam steering vector, resulting in beamforming gain as

$$G_m(\Theta_1,\Theta_2)=\left|b_m^H(r_1,\theta_1,\phi_1)b_m(r_2,\theta_2,\phi_2)\right| \quad (6)$$

where $\Theta_i=(r_i,\theta_i,\phi_i)$ for $i=1,2$ denotes the locations corresponding to the focal point of beamforming vector or the user. It was revealed that since the beamforming gain is influenced by the distance of user $r$, near-field beamforming possesses the focusing ability in the distance domain in ULA systems[3], which is the featuring property of near-field beamforming. To investigate the focusing ability of UCA in the distance domain, we assume that the focal point and the user are aligned in the same direction, i.e., $\theta_1=\theta_2$ and $\phi_1=\phi_2$. The focusing ability in distance domain could be captured with the following lemma.

**Lemma 1** When employing the 3D near-field beam steering vector with UCA $a_m(r_1,\theta,\phi)$ as the beamforming vector, the achieved beamforming gain of the user at $(r_2,\theta,\phi)$ could be expressed as

$$G_m(\Theta_1,\Theta_2)=\left|b_m^H(r_1,\theta,\phi)b_m(r_2,\theta,\phi)\right|\approx\left|J_0(|\xi|)\right| \quad (7)$$

where $\xi=\dfrac{\pi R_m^2\sin^2\theta}{2\lambda}\left(\dfrac{1}{r_1}-\dfrac{1}{r_2}\right)$, $J_0(\cdot)$ denotes the zero-order Bessel function of the first kind.

**Proof** Substituting the approximation of $r_m^{(n)}$ in Eq. (4) into Eq. (7), we can obtain

$$\begin{aligned}&G_m(\Theta_1,\Theta_2)\approx\\&\frac{1}{N}\left|\sum_{n=1}^{N}\mathrm{e}^{\mathrm{j}kR_m^2(1-\sin^2\theta\cos^2(\phi-\psi_n))\left(\frac{1}{2r_1}-\frac{1}{2r_2}\right)}\right|\overset{(a)}{=}\\&\frac{1}{N}\left|\sum_{n=1}^{N}\mathrm{e}^{\mathrm{j}kR_m^2\sin^2\theta\cos(2\phi-2\psi_n)\left(\frac{1}{4r_1}-\frac{1}{4r_2}\right)}\right|\end{aligned} \quad (8)$$

where Eq. (8) is derived by extracting terms independent of $n$ and $\cos^2 x=\dfrac{1+\cos 2x}{2}$. Then, the Jacobi-Anger expansion of Bessel functions could be employed to simplify the equation, expressed as

$$\mathrm{e}^{\mathrm{j}\beta\cos\gamma}=\sum_{s=-\infty}^{+\infty}\mathrm{j}^s\,J_s(\beta)\,\mathrm{e}^{\mathrm{j}s\gamma} \quad (9)$$

where $J_s(\cdot)$ denotes the $s$-order Bessel function of the first kind. By substituting Eq. (9) into Eq. (8), we can obtain

$$G_m(\Theta_1,\Theta_2)=\frac{1}{N}\left|\sum_{s=-\infty}^{+\infty}\mathrm{j}^s\,J_s(\xi)\,\mathrm{e}^{\mathrm{j}2s\phi}\sum_{n=1}^{N}\mathrm{e}^{-\mathrm{j}2s\psi_n}\right| \quad (10)$$

where $\xi=\dfrac{\pi R_m^2\sin^2\theta}{2\lambda}\left(\dfrac{1}{r_1}-\dfrac{1}{r_2}\right)$. Then, the summation over $n$ could be expressed as the piecewise function as

$$\sum_{n=1}^{N}\mathrm{e}^{-\mathrm{j}2s\psi_n}=\begin{cases}N, & s=N/2\cdot t,\ t\in\mathbb{Z};\\ 0, & s\neq N/2\cdot t,\ t\in\mathbb{Z}\end{cases} \quad (11)$$

It can be seen that the piecewise function equals zero except on integral multiples of $N/2$. It was shown that $|J_{|s|}(x)|$ could be assumed negligible for $s=N/2\cdot t$ with $t\neq 0$ and large $N$, which has been commonly adopted in UCA beamforming analysis[18]. Then, due to the symmetry of $J_0(x)$, the equation in Eq. (10) could be finally simplified into

$$G_m(\Theta_1, \Theta_2) \approx \left| J_0\left( \frac{\pi R_m^2 \sin^2\theta}{2\lambda} \left| \frac{1}{r_1} - \frac{1}{r_2} \right| \right) \right| \tag{12}$$

which completes the proof. ■

**Remark 1** Due to the fluctuant but overall downtrend of $|J_0(x)|$ as $x$ scales up, larger distances between the beam focal point and the user will lead to smaller beamforming gain, which reflects the focusing ability of near-field beams in the distance domain. Compared with 2D UCA beamforming in Ref. [9], it can be seen that the elevation angle $\theta$ imposes additional impacts on the beamforming gain. Specifically, if the user is located in the same plane of UCA, i.e., $\theta = \pi/2$, the result in Lemma 1 degrades into the 2D case[9]. Otherwise, if $\theta$ deviates from $\pi/2$, the argument of $J_0(\cdot)$ will be smaller, reducing the impact of the difference in distances $\left| \frac{1}{r_1} - \frac{1}{r_2} \right|$. In other words, the focusing ability of UCA in the distance domain will be weakened near the broadside of UCA (the direction perpendicular to UCA, i.e., $\theta$ is around 0 or $\pi$). This property could not be observed in 2D analysis of UCA near-field beamforming.

To further reveal the significant change of beamforming property from 2D to 3D in UCA systems, the near-field region measured by effective Rayleigh distance (ERD) is compared. According to Ref. [4], ERD could describe the near-field region more accurately compared with the classical Rayleigh distance, defined as the maximum distance where far-field beamforming results in loss exceeding the threshold $\delta$, written as

$$r_{\mathrm{ERD}} \triangleq \arg\max_r \left\{ 1 - \left| b_m^H(r, \theta, \phi) a_m(\theta, \phi) \right| \geqslant \delta \right\} \tag{13}$$

Then, the 3D ERD of UCA could be captured with following corollary.

**Corollary 1** The ERD of UCA in direction $(\theta, \phi)$ could be written as

$$r_{\mathrm{ERD}}^{\mathrm{UCA}}(\theta, \phi) \approx \frac{\pi R_m^2 \sin^2\theta}{2\lambda J_0^{-1}(1-\delta)} \tag{14}$$

where $J_0^{-1}(x) = \left\{ \arg\min_y |J_0(y)| = x \right\}$ returns the minimum $y$ satisfying $|J_0(y)| = x$ for $x \in [0, 1]$.

**Proof** Recall that the far-field beam steering vector $a_m(\theta, \phi)$ can be viewed as a special case of $b_m(r, \theta, \phi)$ when $r \to \infty$. Thus, the ERD could be easily derived by calculating $r_1$ with $r_2 \to \infty$ in Eq. (12), which completes the proof. ■

It is shown in Eq. (14) that the ERD is independent of azimuth angle $\phi$ and proportional to $\sin^2\theta$. Thus, the near-field region dramatically shrinks in the broadside of UCA. When $\theta = 0$ or $\theta = \pi$ is assumed, the ERD tends to zero, revealing that the far-field planar-wave propagation is always accurate and there is no need to consider spherical-wave models in this direction. The reason lies in that, the phase term of waves impinging on different antennas always remains the same from the broadside (perpendicular) direction, no matter planar-wave or spherical-wave model is applied, which is consistent with the result in Ref. [10].

However, this phenomenon indicates that the benefits of near-field communications could not be harvested in the broadside direction of UCA. It has been noticed that the communication systems could benefit from near-field propagation models in enhanced channel orthogonality in multi-user communications[7] and finer performance in localization[19], etc. Therefore, an enlarged near-field region is commonly desired to take advantage of the benefits of near-field communications. To address the problem of the limited near-field region in the broadside of UCA, we shall show that UCCA is a promising method to significantly expand the near-field region in the next subsection.

### 3.2 Beamforming with UCCA

Following a similar investigation method, we shall characterize the 3D beamforming gain with UCCA in the distance domain with the beam steering vector defined in Eq. (5).

**Lemma 2** Employing $b(r_1, \theta, \phi)$ as beamforming vector, the achieved beamforming gain at the location $(r_2, \theta, \phi)$ in the same direction could be expressed as

$$G(\Theta_1, \Theta_2) = \left| b^H(r_1, \theta, \phi) b(r_2, \theta, \phi) \right| \approx \frac{1}{N} \left| \sum_{m=1}^{M} \mathrm{e}^{-\mathrm{j}\frac{\pi R_m^2}{\lambda}\left(\frac{1}{r_1} - \frac{1}{r_2}\right)\left(1 - 1/2\sin^2\theta\right)} N_m J_0(\xi) \right| \tag{15}$$

where $\xi$ is samely defined as $\xi = \dfrac{\pi R_m^2 \sin^2\theta}{2\lambda} \left( \dfrac{1}{r_1} - \dfrac{1}{r_2} \right)$.

**Proof** The proof is provided in Appendix A. ■

It can be seen that the beamforming gain is independent of the azimuth angle $\phi$, revealing the fact that UCCA inherits the advantages of UCA to enable uniform beamforming pattern at different azimuth angles. Although the 3D beamforming gain with UCCA has been derived, the summation operator in Eq. (15) makes it hard to obtain the focusing ability of UCCA in the distance domain. To shed light on the

beamforming property of UCCA, we consider two special cases where the closed-form expressions could be obtained, i.e., the broadside direction and the coplane direction of UCCA.

**Corollary 2** When the user is assumed to be in the broadside of UCCA, i.e., $\theta = 0$, with the assumption that $M$ is large, the beamforming gain in Eq. (15) could be simplified into☆

$$G(\Theta_1, \Theta_2) \overset{\theta=0}{\approx} \frac{1}{\zeta}\left|\mathrm{e}^{-\mathrm{j}\zeta} - 1\right| = \frac{|\sin(\zeta/2)|}{\zeta/2} \tag{16}$$

where $\zeta = \dfrac{\pi R_{\max}^2}{\lambda}\left(\dfrac{1}{r_1} - \dfrac{1}{r_2}\right)$.

**Proof** The proof is provided in Appendix B. ■

**Remark 2** Different from UCA where the beamforming gain is independent of distances in the broadside direction shown in Eq. (7), the beamforming gain becomes sensitive to distances in UCCA systems. The underlying reason is that when applying planar-wave models, the phase of impinging waves still remains the same on antennas in UCAs of different radii. On the contrary, the phase of waves on different UCAs is related to the radius of UCA adopting spherical-wave models. Thus, the far-field beamforming assuming the same phased wave fails to characterize the accurate propagation process in UCCA systems, which sets UCCA apart from existing UCA systems. In addition, it is shown that beamforming gain is independent of the number of UCAs $M$ when $M$ is assumed to be large.

As shown in Fig. 2, different from UCA without the focusing ability in the distance domain, UCCA could focus the energy on a desired distance in the broadside direction. The signal energy leaked to other distances can be controlled to avoid severe interferences when different beams are employed to simultaneously serve different users in the same direction. Moreover, according to the periodic zeros of $\sin(x)$, orthogonal beams could also form toward different distances in the same direction, enabling an optimal interference-free communication scenario. The potential benefits of UCCA in multi-user communications are further verified in the simulation section.

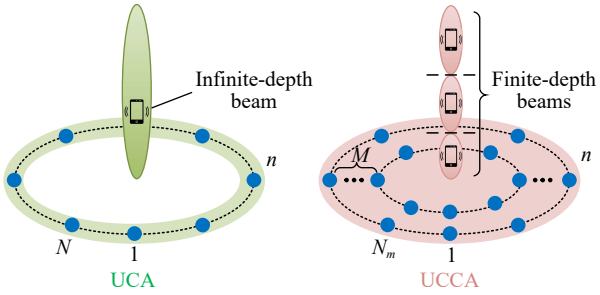


**Fig. 2 Focusing ability comparison in the broadside direction.**

With the beamforming analysis of UCCA, the ERD could be thereby obtained from Eq. (16) as

$$r_{\mathrm{ERD}}^{\mathrm{UCCA}}(0, \phi) = \frac{\pi R_{\max}^2}{2\lambda \Xi^{-1}(1-\delta)} \tag{17}$$

where $\Xi^{-1}(x) = \left\{\arg\min_y \left|\dfrac{\sin y}{y}\right| = x\right\}$. Therefore, compared to the near-zero near-field region of UCA in the broadside direction, it is shown that UCCA is capable of significantly extending the near-field region. Next, the beamforming gain for the second special case is investigated, where users are aligned in the same plane of UCCA.

**Corollary 3** When the user is assumed to be in the same plane of UCCA, i.e., $\theta = \pi/2$, with the assumption that $M$ is large, the beamforming gain in Eq. (15) could be simplified into

$$G(\Theta_1, \Theta_2) \overset{\theta=\pi/2}{\approx} \sqrt{J_0^2(\zeta/2) + J_1^2(\zeta/2)} \tag{18}$$

where $J_1(\cdot)$ denotes the first-order Bessel function of the first kind.

**Proof** The proof is provided in Appendix C. ■

Compared with the 2D beamforming gain for UCA with $G = |J_0(\zeta/2)|$[9], an additional term $J_1(\cdot)$ is introduced for the UCCA scenario. Due to the inequality $\sqrt{J_0^2(\zeta/2) + J_1^2(\zeta/2)} \geqslant |J_0(\zeta/2)|$, the beamforming gain of UCCA exceeds that of UCA with the same $\zeta$. It shows that more energy is leaked in undesired distances at the coplane of UCCA, indicating that the focusing ability of UCCA slightly reduces compared with UCA.

The weakened focusing ability of UCCA will naturally result in the reduction of the near-field region in the same plane of UCCA. To be specific, noting that the ERD could be viewed as the maximum distance where far-field beamforming results in beamforming loss exceeding threshold $\delta$, a stronger focusing ability indicates that the beamforming gain will drop faster and achieve the threshold $\delta$ at a larger distance. As a consequence, a stronger focusing ability leads to a larger near-field region. With this observation, the

☆It is noteworthy that a similar expression of the beamforming gain was derived with a continuous circular array in Ref. [19]. Nevertheless, in this paper we additionally prove that beamforming with a practical discrete UCCA could also converge to the same expression.

weakened focusing ability of UCCA in the coplane would result in the reduction of the near-field region. Intuitively, this reduction originates from that UCCA consists of different-sized UCAs. According to Eq. (14), the near-field region is enlarged with larger UCA. Since the near-field region of UCCA is jointly determined by concentric UCAs with different radii, UCCA's near-field region is smaller than that of UCA with the same radius.

To explicitly compare the beamforming properties of UCA and UCCA, Fig. 3 depicts the comparison between $\sqrt{J_0^2(\zeta/2)+J_1^2(\zeta/2)}$ and $|J_0(\zeta/2)|$. It verifies the correctness of the inequation $\sqrt{J_0^2(\zeta/2)+J_1^2(\zeta/2)} \geqslant |J_0(\zeta/2)|$ and there is no significant deterioration in the focusing ability of UCCA. For instance, when assuming $G=0.8$, the corresponding $\zeta$ for UCA is only 31% smaller compared with that of UCCA. According to the definition of ERD in Eq. (13), it is equivalent to a 31% reduction of the ERD of UCCA compared with UCA in the coplane direction.

To sum up, it can be inferred from the two special cases that, UCCA could significantly increase the focusing ability *near the broadside direction* at the cost of reduced focusing ability *near the coplane* direction.

## 4 Simulation Result

In this section, simulation results are provided to validate the effectiveness of the theoretical analysis. We consider a downlink narrowband mmWave communication with carrier frequency $f_c = 30$ GHz. BS is equipped with UCA or UCCA while the user is assumed to be with a single antenna.

To validate the analysis of 3D beamforming with UCA in Section 3.1, we first assume that the BS is equipped with a 600-element UCA to serve single-antenna users. The user is located at $(r, \pi/3, 0)$ with a variable $r$ while the focal point of the near-field beam is fixed at $(15\,\text{m}, \pi/3, 0)$. As illustrated in Fig. 4, the accurately calculated beamforming gain agrees well with the approximation in Eq. (7), although in the very near region the peaks and valleys do not strictly match. The approximation error in the very near region mainly originates from the inaccurate Taylor series expansion in Eq. (4).

To broaden the near-field region in the broadside direction, we consider a UCCA at BS to replace UCA. To ensure a same array aperture, the number of antennas on the outermost UCA is also set to $N_M = 600$, with $M = 20$. The results in Corollaries 2 and 3 are verified in Fig. 5. The focal points of near-field beams are $(15\,\text{m}, 0, 0)$ and $(15\,\text{m}, \pi/2, 0)$, respectively. It can be seen that UCCA indeed possesses the focusing ability even in the broadside direction, indicating an enlarged near-field region of UCCA compared with UCA.

The near-field region against elevation angle $\theta$ for UCA and UCCA are compared in Fig. 6. The array setup remains the same as in Figs. 4 and 5. The threshold is set to $\delta = 0.2$. Due to the rotational symmetry of UCA or UCCA, the near-field region is independent of azimuth angle $\phi$. Thus, only the relationship between ERD and elevation angle $\theta$ is investigated. It is shown that, the estimated ERD for UCA with Eq. (14) could achieve good estimation accuracy on the whole, confirming the near-zero near-field region in the broadside of UCA. When $\theta$ approaches the broadside direction 0 or $\pi$, the estimated beamforming gain slightly deviates from the accurate value, which also results from the inaccurate

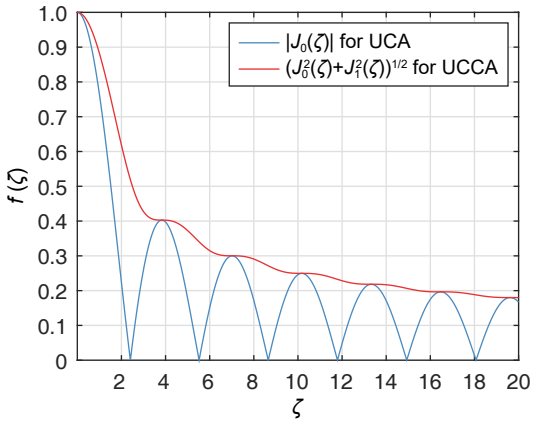


**Fig. 3 Comparing the beamforming gain of UCA and UCCA assuming $\theta = \pi/2$.**

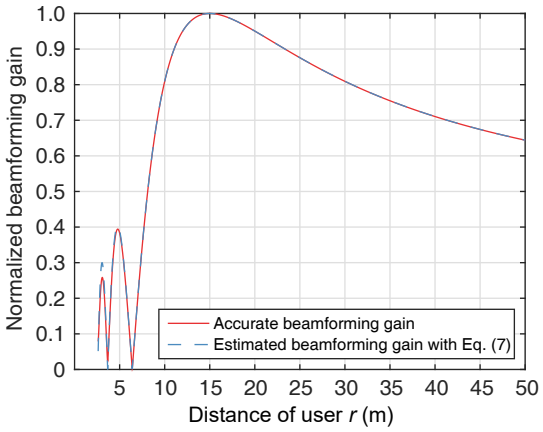


**Fig. 4 3D beamforming gain with UCA.**

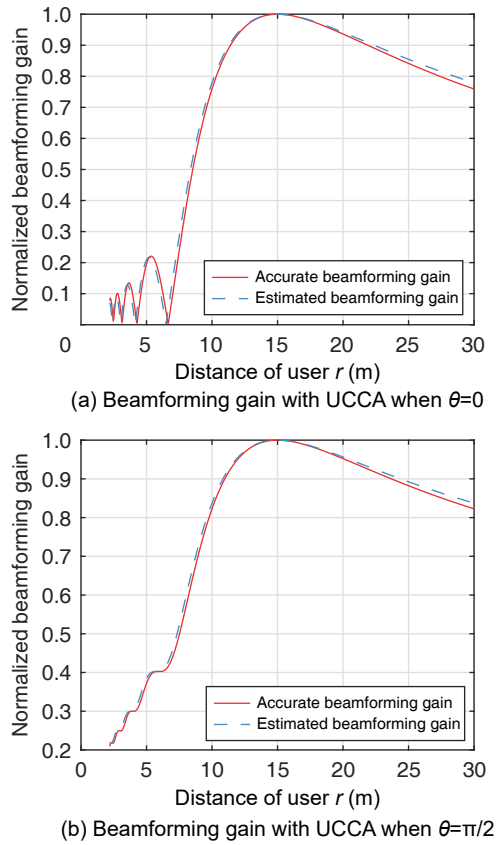


**Fig. 5 Verification of the beamforming gain in directions of $\theta = 0$ and $\theta = \pi/2$.**

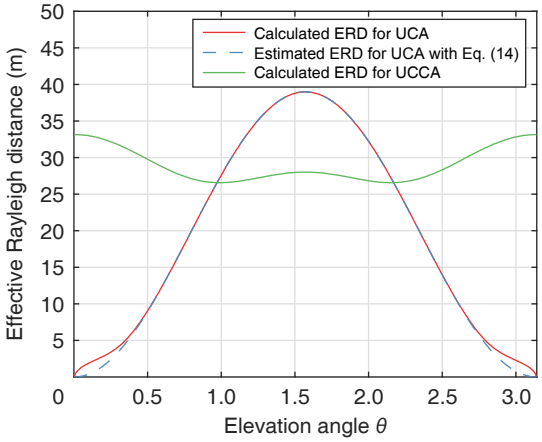


**Fig. 6 Near-field region measured by ERD for UCCA and UCA.**

approximation of the distance term in Eq. (4) in very near regions. In addition, as discussed in Section 3.2, it also verifies that UCCA acquires stronger focusing ability near the broadside direction and slightly weakened focusing ability near the coplane space. The reduction of the near-field region of UCCA in the coplane is about 30%, which is consistent with the theoretical analysis. The intersection point of the near-field region, indicating that UCCA and UCA possess the same focusing ability, is about $0.3\pi$ in this simulation.

Furthermore, to reveal the potential of UCCA to improve the spectrum efficiency in hybrid precoding schemes by enhancing multi-user channel orthogonality, a simulation of the spectrum efficiency against the number of users is performed. In this simulation, $N_M = 1200$ and $M = 20$ are assumed and single-antenna users are aligned in the $z$-axis within the range [4 m, 40 m]. A multi-path channel is assumed which consists of one LoS path and $L = 2$ non-line-of-sight (NLoS) paths. The energy of LoS components is assumed to be 10 dB larger than the NLoS components. We follow a hybrid precoding design method similar to Section V-A in Ref. [7], where the matched filter of the beam steering vector of LoS path is selected as the analog precoding to maximize the received power. The digital precoder is designed according to the zero-forcing method. We consider two distribution scenarios, i.e., the users are randomly located in the same direction and optimally located at zeros of other beams with only the LoS path, which could support perfect orthogonal transmissions according to property of the sinc function in Eq. (16). As shown in Fig. 7, UCCA could enhance the spectrum efficiency for both scenarios when the number of users is less than 5, while the performance of optimally located users continues to scale up when the number of users is less than 8. The black dashed line denotes the far-field scenario, where only one user could be served. Therefore, this figure illustrates that the enlarged near-field region of UCCA could be leveraged to enhance the performance of multi-user communications in practical multi-path scenarios. It is worth noting that

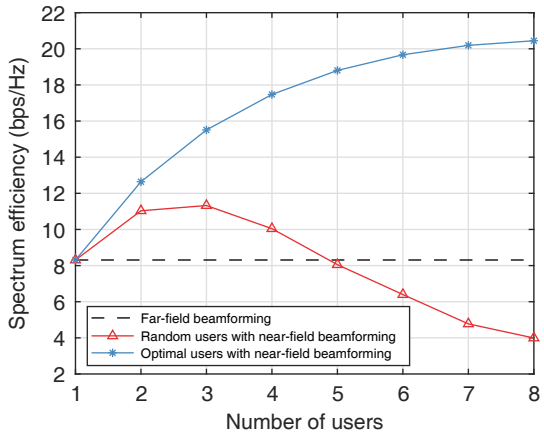


**Fig. 7 Spectrum efficiency in multi-user communications with UCCA.**

since the near-field region of UCA is near zero in broadside directions, UCA could only perform far-field beamforming in such direction, which could not benefit from such performance enhancement.

## 5 Conclusion

In this paper, enhanced focusing ability of UCCA is investigated. The 3D beamforming gain and near-field region with UCA are characterized in closed form, revealing the phenomenon of limited near-field region in the broadside direction of UCA. In addition to the benefits of higher space utilization efficiency of UCCA, we explore the possibility of UCCA in generating an enlarged near-field region in broadside direction. Compared with UCA, UCCA is capable of producing a more uniform near-field region at different elevation angles. The enlarged near-field region is verified to be beneficial for performance enhancement in multi-user communications. Based on the beamforming property of UCCA, an efficient beam-steering-based codebook with UCCA could be designed and is left for future research.

### Acknowledgment

This work was supported by the National Natural Science Foundation of China (No. 62031019) and the European Commission through the H2020-MSCA-ITN META WIRELESS Research Project (No. 956256).

## Appendix

### A Proof of Lemma 2

By substituting the approximated distance term in Eq. (4), the Eq. (15) could be rewritten as

$$G(\Theta_1,\,\Theta_2)=\left|b^H(r_1,\,\theta,\,\phi)b^H(r_2,\,\theta,\,\phi)\right|=\frac{1}{N}\left|\sum_{m=1}^{M}\sum_{n=1}^{N_m}\mathrm{e}^{-\mathrm{j}k\frac{R_m^2}{2}\left(1-\sin^2\theta\cos^2(\phi-\psi_n)\right)\left(\frac{1}{r_1}-\frac{1}{r_2}\right)}\right| \tag{A1}$$

where the two summations are derived from different UCAs and different antennas on each UCA. Then, we separate the terms in Eq. (A1) into two terms dependent and independent of $n$, which is expressed as

$$G(\Theta_1,\Theta_2)\overset{(a)}{=}\frac{1}{N}\left|\sum_{m=1}^{M}\mathrm{e}^{-\mathrm{j}k\frac{R_m^2}{2}\left(\frac{1}{r_1}-\frac{1}{r_2}\right)(1-1/2\sin^2\theta)}\times\sum_{n=1}^{N_m}\mathrm{e}^{\mathrm{j}k\frac{R_m^2\sin^2\theta}{4}\cos(2\phi-2\psi_n)\left(\frac{1}{r_1}-\frac{1}{r_2}\right)}\right| \tag{A2}$$

where (a) is derived with the double-angle formulae $\cos^2(x)=\frac{1}{2}(1+\cos(2x))$. Then, following a similar process in Lemma 1, the term in the summation of $n$ could be simplified as

$$\sum_{n=1}^{N_m}\mathrm{e}^{\mathrm{j}k\frac{R_m^2\sin^2\theta}{4}\cos(2\phi-2\psi_n)\left(\frac{1}{r_1}-\frac{1}{r_2}\right)}=\sum_{s=-\infty}^{+\infty}j^sJ_s(\xi)\mathrm{e}^{\mathrm{j}2s\phi}\sum_{n=1}^{N_m}\mathrm{e}^{-\mathrm{j}2s\psi_n}\approx N_mJ_0(\xi) \tag{A3}$$

where $\xi=\dfrac{\pi R_m^2\sin^2\theta}{2\lambda}\left(\dfrac{1}{r_1}-\dfrac{1}{r_2}\right)$. Finally, the beamforming gain in Eq. (15) could be obtained by substituting the approximation in Eq. (A3), which completes the proof. ■

### B Proof of Corollary 2

First, we reformulate all the parameters in forms of $m$, expressed as

$$R_m=\frac{m}{M}R_{\max},\quad N_m=\frac{4\pi R_{\max}}{\lambda M}m,\quad N=\sum_{m=1}^{M}\frac{4\pi R_{\max}}{\lambda M}m=\frac{2\pi(M+1)R_{\max}}{\lambda} \tag{A4}$$

Then, with the knowledge of $\theta=0$ and $J_0(0)=1$, Eq. (15) could be rewritten as

$$G(\Theta_1,\Theta_2)\approx\frac{1}{N}\left|\sum_{m=1}^{M}N_m\mathrm{e}^{-\mathrm{j}\frac{\pi R_m^2}{\lambda}\left(\frac{1}{r_1}-\frac{1}{r_2}\right)}\right|\overset{(a)}{=}\frac{2}{M(M+1)}\left|\sum_{m=1}^{M}m\mathrm{e}^{-\mathrm{j}\zeta\frac{m^2}{M^2}}\right| \tag{A5}$$

where $\zeta=\dfrac{\pi R_{\max}^2}{\lambda}\left(\dfrac{1}{r_1}-\dfrac{1}{r_2}\right)$ and (a) is derived by substituting Eq. (A4) into Eq. (15). Since a large $M$ is assumed, the summation could be well approximated with the integral. Thus, the beamforming gain could be further simplified into

$$G(\Theta_1,\Theta_2)\approx\frac{2}{M(M+1)}\left|\int_0^M m\mathrm{e}^{-\mathrm{j}\zeta\frac{m^2}{M^2}}\mathrm{d}m\right|\overset{(b)}{=}\frac{M}{(M+1)}\frac{1}{\zeta}\left|\mathrm{e}^{-\mathrm{j}\zeta}-1\right|\overset{(c)}{\approx}\frac{1}{\zeta}\left|\mathrm{e}^{-\mathrm{j}\zeta}-1\right|=\frac{2\left|\sin\left(\frac{\zeta}{2}\right)\right|}{\zeta} \tag{A6}$$

where (b) is derived with the integral $\int x\mathrm{e}^{\mathrm{j}ax^2}\mathrm{d}x=\dfrac{1}{2\mathrm{j}a}\mathrm{e}^{\mathrm{j}ax^2}$ and approximation (c) is derived by assuming

$\frac{M}{M+1} \approx 1$. This completes the proof. ■

## C Proof of Corollary 3

By substituting Eq. (A4) into Eq. (15) and employing the assumption $\theta = \pi/2$, the beamforming gain could be rewritten as

$$G(\Theta_1,\Theta_2) \overset{\theta=\pi/2}{\approx} \frac{1}{N}\left|\sum_{m=1}^{M} \mathrm{e}^{-\mathrm{j}\xi} N_m J_0(\xi)\right| = \frac{2}{M(M+1)}\left|\sum_{m=1}^{M} m\mathrm{e}^{-\mathrm{j}\frac{\zeta}{2M^2}m^2} J_0\left(\frac{\zeta}{2M^2}m^2\right)\right| \tag{A7}$$

where $\zeta$ is samely defined as $\zeta = \frac{\pi R_{\max}^2}{\lambda}\left(\frac{1}{r_1}-\frac{1}{r_2}\right)$. When assuming $M$ is very large, we could replace the intractable summation with integral, refomulating the equation into

$$\begin{aligned} G(\Theta_1,\Theta_2) &\approx \frac{1}{N}\left|\sum_{m=1}^{M} \mathrm{e}^{-\mathrm{j}\xi} N_m J_0(\xi)\right| \approx \\ &\frac{2}{M(M+1)}\left|\int_0^M x\mathrm{e}^{-\mathrm{j}\frac{\zeta}{2M^2}x^2} J_0\left(\frac{\zeta}{2M^2}x^2\right)\mathrm{d}x\right| = \\ &\frac{2}{M(M+1)}\frac{2M^2}{\zeta}\left|\int_0^{\sqrt{\zeta/2}} x\mathrm{e}^{-\mathrm{j}x^2} J_0(x^2)\mathrm{d}x\right| \end{aligned} \tag{A8}$$

Then, the integral is addressed by separately considering the real and imaginary part. The real part of the integral is expressed as

$$\begin{aligned} &\mathcal{R}\left\{\int_0^{\sqrt{\zeta/2}} x\mathrm{e}^{-\mathrm{j}x^2} J_0(x^2)\mathrm{d}x\right\} = \\ &\int_0^{\sqrt{\zeta/2}} x\cos(x^2) J_0(x^2)\mathrm{d}x = \\ &\frac{1}{2}x^2\left(\sin x^2 J_1(x^2) + \cos x^2 J_0(x^2)\right) \end{aligned} \tag{A9}$$

Similarly, the imaginary part could be expressed as

$$\begin{aligned} &\mathcal{I}\left\{\int_0^{\sqrt{\zeta/2}} x\mathrm{e}^{-\mathrm{j}x^2} J_0(x^2)\mathrm{d}x\right\} = \\ &-\mathrm{j}\int_0^{\sqrt{\zeta/2}} x\sin(x^2) J_0(x^2)\mathrm{d}x = \\ &-\frac{1}{2}\mathrm{j}x^2\left(\sin x^2 J_0(x^2) - \cos x^2 J_1(x^2)\right) \end{aligned} \tag{A10}$$

Thus, the absolute of the integral could be simplified into

$$\left|\int_0^{\sqrt{\zeta/2}} x\mathrm{e}^{-\mathrm{j}x^2} J_0(x^2)\mathrm{d}x\right| = \frac{1}{2}x^2\sqrt{J_0^2(x^2)+J_1^2(x^2)} \tag{A11}$$

With the results of integral, the beamforming gain in Eq. (A8) could be rewritten as

$$G(\Theta_1,\Theta_2) \approx \sqrt{J_0^2(\zeta/2)+J_1^2(\zeta/2)} \tag{A12}$$

which completes the proof. ■

## References


[1] H. Lu and Y. Zeng, Communicating with extremely large-scale array/surface: Unified modeling and performance analysis, *IEEE Trans. Wirel. Commun.*, vol. 21, no. 6, pp. 4039–4053, 2022.

[2] M. Cui, Z. Wu, Y. Lu, X. Wei, and L. Dai, Near-field MIMO communications for 6G: Fundamentals, challenges, potentials, and future directions, *IEEE Commun. Mag.*, vol. 61, no. 1, pp. 40–46, 2023.

[3] E. Bjornson, O. T. Demir, and L. Sanguinetti, A primer on near-field beamforming for arrays and reconfigurable intelligent surfaces, in *Proc. 2021 55th Asilomar Conf. Signals, Systems, and Computers*, Pacific Grove, CA, USA, 2021, pp. 105–112.

[4] M. Cui and L. Dai, Near-field wideband beamforming for extremely large antenna arrays, arXiv preprint arXiv: 2109.10054, 2021.

[5] H. Zhang, N. Shlezinger, F. Guidi, D. Dardari, and Y. C. Eldar, 6G wireless communications: From far-field beam steering to near-field beam focusing, *IEEE Commun. Mag.*, vol. 61, no. 4, pp. 72–77, 2023.

[6] H. Zhang, N. Shlezinger, F. Guidi, D. Dardari, M. F. Imani, and Y. C. Eldar, Beam focusing for near-field multiuser MIMO communications, *IEEE Trans. Wirel. Commun.*, vol. 21, no. 9, pp. 7476–7490, 2023.

[7] Z. Wu and L. Dai, Multiple access for near-field communications: SDMA or LDMA? *IEEE J. Select. Areas Commun.*, vol. 41, no. 6, pp. 1918–1935, 2023.

[8] V. Kallnichev, Analysis of beam-steering and directive characteristics of adaptive antenna arrays for mobile communications, *IEEE Antennas Propag. Mag.*, vol. 43, no. 3, pp. 145–152, 2001.

[9] Z. Wu, M. Cui, and L. Dai, Enabling more users to benefit from near-field communications: From linear to circular array, arXiv preprint arXiv: 2212.14654, 2022.

[10] Y. Xie, B. Ning, L. Li, and Z. Chen, Near-field beam training in THz communications: The merits of uniform circular array, *IEEE Wirel. Commun. Lett.*, vol. 12, no. 4, pp. 575–579, 2023.

[11] S. C. Chan and H. H. Chen, Uniform concentric circular arrays with frequency-invariant characteristics—Theory, design, adaptive beamforming and DOA estimation, *IEEE Trans. Signal Process.*, vol. 55, no. 1, pp. 165–177, 2007.

[12] M. Mahmood, A. Koc, and T. Le-Ngoc, 2D antenna array structures for hybrid massive MIMO precoding, in *Proc. GLOBECOM 2020-2020 IEEE Global Communications Conference*, Taipei, China, 2020.

[13] G. Huang, J. Chen, and J. Benesty, Insights into frequency-invariant beamforming with concentric circular microphone arrays, *IEEE/ACM Trans. Audio Speech Lang. Process.*, vol. 26, no. 12, pp. 2305–2318, 2018.

[14] O. El Ayach, S. Rajagopal, S. Abu-Surra, Z. Pi, and R. W.

Heath, Spatially sparse precoding in millimeter wave MIMO systems, *IEEE Trans. Wirel. Commun.*, vol. 13, no. 3, pp. 1499–1513, 2014.

[15] K. T. Selvan and R. Janaswamy, Fraunhofer and Fresnel Distances: Unified derivation for aperture antennas, *IEEE Antennas Propag. Mag.*, vol. 59, no. 4, pp. 12–15, 2017.

[16] M. Cui and L. Dai, Channel estimation for extremely large-scale MIMO: Far-field or near-field? *IEEE Trans. Commun.*, vol. 70, no. 4, pp. 2663–2677, 2022.

[17] F. Zhang, W. Fan, and G. F. Pedersen, Frequency-invariant uniform circular array for wideband mm-wave channel characterization, *IEEE Antennas Wirel. Propag. Lett.*, vol. 16, pp. 641–644, 2017.

[18] D. Dardari, N. Decarli, A. Guerra, and F. Guidi, LOS/NLOS near-field localization with a large reconfigurable intelligent surface, *IEEE Trans. Wirel. Commun.*, vol. 21, no. 6, pp. 4282–4294, 2022.

[19] A. Kosasih and E. Bjornson, Finite beam depth analysis for large arrays, arXiv preprint arXiv: 2306.12367, 2023.

**Linglong Dai** received the BS degree from Zhejiang University, Hangzhou, China, in 2003, the MS degree from the China Academy of Telecommunications Technology, Beijing, China, in 2006, and the PhD degree from Tsinghua University, Beijing, in 2011. From 2011 to 2013, he was a postdoctoral researcher with Department of Electronic Engineering, Tsinghua University, where he was an assistant professor from 2013 to 2016, an associate professor from 2016 to 2022, and has been a professor since 2022. His current research interests include massive MIMO, reconfigurable intelligent surface (RIS), mmWave and Terahertz communications, wireless AI, and electromagnetic information theory. He received the National Natural Science Foundation of China for Outstanding Young Scholars in 2017, the IEEE ComSoc Leonard G. Abraham Prize in 2020, the IEEE ComSoc Stephen O. Rice Prize in 2022, the IEEE ICC Outstanding Demo Award in 2022, and the National Science Foundation for Distinguished Young Scholars in 2023. He was listed as a Highly Cited Researcher by Clarivate from 2020 to 2023. He was elevated as an IEEE Fellow in 2022.

**Zidong Wu** received the BEng degree in electronic engineering from Tsinghua University, Beijing, China, in 2019. He is currently pursuing the PhD degree in Department of Electronic Engineering at Tsinghua University, Beijing, China. His research interests include massive MIMO, mmWave communications, machine learning for wireless communications, and near-field communications. He has received the Honorary Mention of IEEE ComSoc Student Competition in 2019 and IEEE ICC Oustanding Demo Award in 2022.